Inorganic Chemistry
Article
Cite This: Inorg. Chem. XXXX, XXX, XXX−XXX
pubs.acs.org/IC

Light-Driven Water Oxidation with the Ir-blue Catalyst and the $Ru(bpy)_3^{2+}/S_2O_8^{2-}$ Cycle: Photogeneration of Active Dimers, Electron-Transfer Kinetics, and Light Synchronization for Oxygen Evolution with High Quantum Efficiency

Andrea Volpe,[†] Cristina Tubaro,[†] Mirco Natali,[*,‡] Andrea Sartorel,[*,†] Gary W. Brudvig,[§] and Marcella Bonchio[†]

[†]Department of Chemical Sciences, University of Padova, via Marzolo 1, 35131 Padova, Italy

[‡]Department of Chemical and Pharmaceutical Sciences, University of Ferrara and Centro Interuniversitario per la Conversione Chimica dell'Energia Solare (SolarChem), sez. di Ferrara, via L. Borsari 46, 44121 Ferrara, Italy

[§]Department of Chemistry, Yale University, 225 Prospect Street, New Haven, Connecticut 06520-8107, United States

Supporting Information

ABSTRACT: Light-driven water oxidation is achieved with the $Ru(bpy)_3^{2+}/S_2O_8^{2-}$ cycle employing the highly active **Ir-blue** water oxidation catalyst, namely, an $Ir^{IV,IV}_2(pyalc)_2$ μ-oxo-dimer [pyalc = 2-(2′-pyridyl)-2-propanoate]. **Ir-blue** is readily formed by stepwise oxidation of the monomeric Ir(III) precursor **1** by the photogenerated $Ru(bpy)_3^{3+}$, with a quantum yield ϕ of up to 0.10. Transient absorption spectroscopy and kinetic evidence point to a stepwise mechanism, where the primary event occurs via a fast photoinduced electron transfer from **1** to $Ru(bpy)_3^{3+}$, leading to the Ir(IV) monomer $\mathbf{I_1}$ ($k_1 \sim 10^8$ M^{-1} s^{-1}). The competent **Ir-blue** catalyst is then obtained from $\mathbf{I_1}$ upon photooxidative loss of the Cp* ligand and dimerization. The **Ir-blue** catalyst is active in the $Ru(bpy)_3^{2+}/S_2O_8^{2-}$ light-driven water oxidation cycle, where it undergoes two fast photoinduced electron transfers to $Ru(bpy)_3^{3+}$ [with $k_{\text{Ir-blue}} = (3.00 \pm 0.02) \times 10^8$ M^{-1} s^{-1} for the primary event, outperforming iridium oxide nanoparticles by ca. 2 orders of magnitude], leading to a $Ir^{V,V}_2$ steady-state intermediate involved in O−O bond formation. The quantum yield for oxygen evolution depends on the photon flux, showing a saturation regime and reaching an impressive value of $\phi(O_2) = 0.32 \pm 0.01$ (corresponding to a quantum efficiency of 64 ± 2%) at low irradiation intensity. This result highlights the key requirement of orchestrating the rate of the photochemical events with dark catalytic turnover.

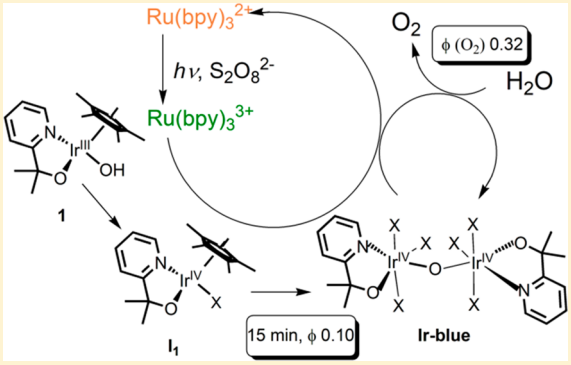

INTRODUCTION

Light-driven water oxidation catalysis is still posing one formidable challenge for the production of solar fuels by artificial photosynthesis.[1−3] The major hurdle comes from a proper matching of light-induced charge-separation events with the dark, catalytic, four-electron water-to-dioxygen conversion. This latter transformation often exploits multi-redox catalytic manifolds, which can drive the process at minimal overpotential and with fast kinetics. Despite the low abundance and high cost of Ir, Ir-based water oxidation catalysts (WOCs) are receiving increasing attention because of their unique performance.[4−8] In particular, the Ir(IV,IV) mono-μ-oxo dimers (**Ir-blue**) stabilized by 2-(2′-pyridyl)-2-propanoate (pyalc),[9] stand out as superior molecular WOCs, exhibiting (i) minimal overpotential (η < 15 mV),[10] approaching the thermodynamic value of the O_2/H_2O couple, (ii) activity over the quasi-entire pH range (1−13), (iii) millions of turnover numbers (TONs; >10^6),[10] (iv) one of the fastest turnover frequencies (TOFs) available so far (up to 8 s^{-1}),[10,11] and (v) facile surface chemisorption onto a photoelectrode for regenerative water-splitting applications.[10,12−16] One winning feature is the ability of the **Ir-blue** manifold to access high-valent, contiguous Ir(IV,IV) and Ir(IV,V) states,[17,18] by virtue of the strong electron-donating effect of the robust pyalc ligand. Evidence for the evolution of the Ir(III) monomeric precursor **1** to the catalytically active Ir(IV,IV) blue dimer has been obtained by chemical or electrochemical methods, which can affect the oxidative loss of the pentamethylcyclopentadienyl (Cp*) ancillary ligand and dimer formation (Scheme 1, top). In particular, the nature and composition of the **Ir-blue** dimers, including a high number of geometrical isomers,[19] are conveniently probed by a UV−vis fingerprint centered at 588−620 nm.[10,20,21] In all cases, the

Received: August 21, 2019

DOI: 10.1021/acs.inorgchem.9b02531
Inorg. Chem. XXXX, XXX, XXX−XXX

Scheme 1. Generation of Ir-blue WOC by Overnight Dark Chemical/Electrochemical Oxidation of the Mononuclear Ir(III) Precursor 1, Featuring Cp* and pyalc Bidentate Ligands (Top, Current Methods),[10,11,20,21] and Fast Photochemical Activation of 1 to Ir-blue in ca. 15 min and with $\phi_{\text{Ir-blue}}$ of up to 0.10, within the $Ru(bpy)_3^{2+}/Na_2S_2O_8$ System (Bottom, This Work), through the Formation of a Monomeric Ir(IV) Intermediate I_1[a]

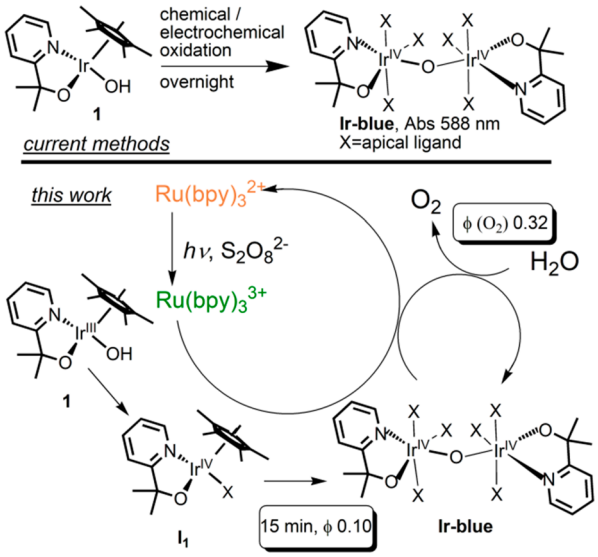

[a]The **Ir-blue** WOC enables then photochemical water oxidation to oxygen with $\phi(O_2)$ of up to 0.32. See the details in Scheme S1.

WOC activity of **Ir-blue** has been mainly investigated under dark electrocatalytic conditions[11] or by the use of bulk chemical oxidants such as Ce(IV) or $NaIO_4$.[22] In this work, we address light-induced water oxidation by **Ir-blue** within the $Ru(bpy)_3^{2+}$ (bpy = 2,2′-bipyridine)/$S_2O_8^{2-}$ photoactivated cycle, starting from **1** as the Ir precursor (Scheme 1, bottom). Light activation provides a new capability for time-resolved measurements to probe the mechanism, by characterization of intermediates and electron-transfer kinetics. Photogeneration of **Ir-blue** occurs from **1** at the initial stage of the process, thus forming the competent WOC in aqueous solution, which is responsible for continuous photoassisted oxygen evolution. In this notion, the direct light-energy conversion into new chemical bonds yielding functional light-harvesting/catalytic systems for water splitting is the core mission of artificial photosynthesis research for sustainable energy.[15,16,23,24] Our results include (i) kinetic evidence on the stepwise evolution of the precatalyst **1** into the catalytically active **Ir-blue** species, which occurs in aqueous solution upon visible-light irradiation of the **1**/$Ru(bpy)_3^{2+}/S_2O_8^{2-}$ system (Scheme 1), (ii) transient absorption spectroscopy evidence of a primary Ir(IV) mononuclear intermediate ($\mathbf{I_1}$), formed from one-electron oxidation of **1** by Ru(III), (iii) dynamic mapping by flash photolysis of Ir-to-Ru(III) electron-transfer kinetics along the conversion of **1** into **Ir-blue**, (iv) photoassisted oxygen evolution kinetics catalyzed by **Ir-blue**, showing a light-dictated limiting regime at low photon flux, and (v) a change to the chemical rate-determining step at high photon flux, which is likely related to O−O bond formation by a high-valent $Ir^{V,V}_2$ intermediate. The latter experiments confirm that tuning the light intensity in relation to the catalytic rate is pivotal in order to maximize the photocatalytic efficiency.[25,26]

RESULTS AND DISCUSSION

Photogeneration of Ir-blue under Visible Light. Few Ir(III) precatalysts, bearing the Cp* ligand together with chelating donors, have been used in combination with the $Ru(bpy)_3^{2+}$ photosensitizer and the persulfate anion, $S_2O_8^{2-}$, as the sacrificial electron acceptor (Scheme S1).[26−30] In these photocatalytic cycles, photogenerated $Ru(bpy)_3^{3+}$ is expected to drive oxidation of the Ir precursor up to the high-valent dinuclear Ir WOC species (**Ir-blue**) responsible for oxygen evolution (Scheme 1). Importantly, a stepwise oxidation of the Ir(III) precursor has been postulated, but identification of the competent WOC still remains elusive.

When a solution of 1 mM $Ru(bpy)_3^{2+}$ and 5 mM $Na_2S_2O_8$ in 50 mM $Na_2SiF_6/NaHCO_3$ buffer at pH = 5.2 [the $Na_2SiF_6/NaHCO_3$ buffer is often used in light-driven catalysis with $Ru(bpy)_3^{2+}$ because of the good stability of the Ru(III) state[31−34]] is irradiated with white light (3.8 mW cm^{-2}), conversion of $Ru(bpy)_3^{2+}$ into $Ru(bpy)_3^{3+}$ is confirmed by a progressive bleaching of the metal-to-ligand charge-transfer (MLCT) band centered at λ = 450 nm, with a parallel rise of an absorbance at λ = 670 nm and an isosbestic point observed at 568 nm (differential absorption spectra at 0−7 min irradiation are shown in Figure 1, top panel; see full spectra in Figure S1). Monoexponential fitting of the absorbance monitored at both 452 and 670 nm wavelengths provides the first-order kinetic constant of $Ru(bpy)_3^{3+}$ photogeneration, $k_{Ru(III)} = (2.21 \pm 0.15) \times 10^{-2}\ s^{-1}$ (eq 1), under the specific conditions adopted [the initial rate value $R_{0,Ru(III)}$ in eq 2 refers to the initial rate of Ru(III) production, when [Ru(II)] = 1 mM].

$$R_{Ru(III)} = d[Ru(III)]/dt = k_{Ru(III)}[Ru(II)] \quad (1)$$

$$R_{0,Ru(III)} = (2.21 \pm 0.15) \times 10^{-5}\ M\ s^{-1} \quad (2)$$

In the absence of any reducing species, $Ru(bpy)_3^{3+}$ lasts in solution for few minutes, until it self-bleaches upon bpy ligand oxidation.[35−37] Conversely, in the presence of the Ir(III) precatalyst **1**, photogenerated $Ru(bpy)_3^{3+}$ (E = 1.26 vs normal hydrogen electrode, NHE) is responsible for an oxidative cascade that ends up with formation of the **Ir-blue** manifold. Conversion of **1** (50−400 μM) into **Ir-blue** by the light-activated $Ru(bpy)_3^{2+}/S_2O_8^{2-}$ system is indeed confirmed by evolution of the differential absorption spectra in time, showing a broad band centered at λ = 588 nm, which is diagnostic of Ir(IV) dimers (Figures 1, middle panel, and S2 and S3). Under the conditions explored (Figure 1), ΔAbs@588 nm levels off after ca. 15 min of irradiation, with rates and final plateau values that depend on the concentration of the Ir(III) precursor **1**. The intensity of ΔAbs@588 nm at the plateau is fairly consistent with that obtained upon treatment of **1** with an excess of $NaIO_4$ as the chemical oxidant,[11,20,21] suggesting quantitative conversion of **1** into **Ir-blue** in such a time frame. Quantum yields for **Ir-blue** production, defined as the ratio between the amount of **Ir-blue** formed and the absorbed photons, can be estimated in the range $\phi_{\text{Ir-blue}}$ = 0.035−0.10, using photogeneration of Ru(III) as an actinometer. This results (eq 3) from a comparison of the initial rates of **Ir-blue** formation ($R_{0,\text{Ir-blue}}$; see Figure S4) and of Ru(III) photogeneration ($R_{0,Ru(III)}$) previously determined and considering that Ru(III) photogeneration is associated with $\phi_{Ru(III)}$ = 2 [the rate of Ru(III) photogeneration along **Ir-blue** formation under the conditions above can be assumed to be constant and

DOI: 10.1021/acs.inorgchem.9b02531
Inorg. Chem. XXXX, XXX, XXX−XXX

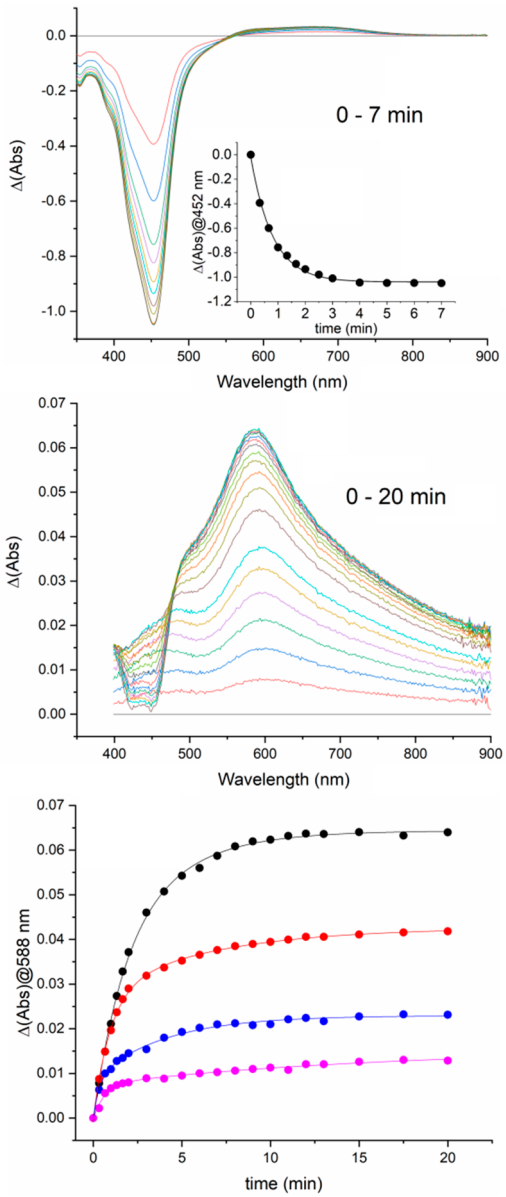

Figure 1. Top: Differential absorbance spectra of a solution containing 1 mM $Ru(bpy)_3^{2+}$ and 5 mM $Na_2S_2O_8$ in 50 mM $Na_2SiF_6/NaHCO_3$ buffer (pH = 5.2) at different times (0–7 min) upon illumination with white light [white LED; 3.8 mW cm^{-2}; optical path of the cuvette = 1 mm]. Inset: Bleaching of the absorbance at 452 nm and related monoexponential fitting. Middle: Differential absorbance spectra under the same conditions but in the presence of 400 μM **1** (0–20 min), as a representative case. Bottom: Plot of the differential absorbance at 588 nm versus time, with **1** = 400 μM (black), 200 μM (red), 100 μM (blue), 50 μM (pink). The lines do not come from fitting of the experimental traces and have been added in order to help visualization of the Δ(Abs) evolution trend; indeed, the ΔAbs@588 nm versus time curves required fitting with biexponential functions (Figure S4), suggesting the occurrence of a complex mechanism involving the intermediates that convert into **Ir-blue**; competitive consumption of a photogenerated $Ru(bpy)_3^{3+}$ oxidant for progressive degradation of the Cp* ligand and for water oxidation could also be responsible for the complex kinetics of **Ir-blue** formation. See the discussion in the main text.

equal to $R_{0,Ru(III)} = (2.21 \pm 0.15) \times 10^{-5}$ M s^{-1} on the basis of a persistent concentration of [Ru(II)] ∼ 1 mM, demonstrated by the negligible bleaching of the absorption at 450 nm (Figure 1, middle panel); the initial rate of **Ir-blue** photogeneration $R_{0,\textbf{Ir-blue}}$ was estimated from a linear fitting of the initial, <2 min, ΔAbs at 588 nm (see Figure S4 and Table S1 for further details).[38,39]

$$\phi_{\textbf{Ir-blue}} = (R_{0,\textbf{Ir-blue}}/R_{0,Ru(III)})\phi_{Ru(III)} \quad (3)$$

As to formation of the **Ir-blue** species by the photogenerated $Ru^{III}(bpy)_3^{3+}$, a stepwise mechanism involving oxidation to Ir(IV), degradation of the Cp* ligand, and dimerization can be envisioned (Scheme S2). To this respect, the apparently low value of $\phi_{\textbf{Ir-blue}}$ might be thus related to the complex mechanistic requirements (Scheme S2). In order to map possible degradation products, experiments were conducted under a degassed atmosphere in a sealed reactor, employing 15 mL of the reaction solutions. Among possible carboxylic acids as degradation products of Cp*,[40−42] 0.13 mM acetic acid was detected by high-performance liquid chromatography for the solution containing 50 μM **1** after 2 h of irradiation, corresponding to 2.6 equiv of acetic acid released per **1** [as a control experiment, irradiating the $Ru(bpy)_3^{2+}/S_2O_8^{2-}$ solution in the absence of **1**, the acetic acid concentration was found to be below 0.01 mM]. Similarly, 1.8 equiv of acetic acid was formed upon decomposition of the Cp* ligand of **1** in the presence of 100 equiv of $NaIO_4$, enabling formation of the active Ir dimer.[21] Conversely, formic acid was not observed as a degradation product of Cp* under irradiation, with its concentration being below the detection limit of 0.01 mM.

Extensive decomposition of Cp* is also required to guarantee the stability of **Ir-blue**. Unstable blue solutions were indeed obtained in the electrochemical generation of **Ir-blue** because of the presence of intermediate oxidation products of the Cp* ring capable of reducing Ir(IV) to Ir(III).[11] On the other hand, in the case of photochemical activation (Figure 1), the **Ir-blue** spectral features are persistent under dark conditions up to several hours, suggesting that sufficient oxidizing equivalents are provided. Indeed, considering a constant rate of Ru(III) photogeneration, $R_{0,Ru(III)} = (2.21 \pm 0.15) \times 10^{-5}$ M s^{-1}, this results in an apparent ∼26 mM Ru(III) production along the 20 min of irradiation, corresponding to 65–520 oxidizing equivalents with respect to **1** (50–400 μM concentration).

As a final note, 3.7 μmol of CO_2 was detected in the headspace in the presence of 50 μM **1** after 2 h of irradiation under the same conditions. However, in this case the blank control [$Ru(bpy)_3^{2+}/S_2O_8^{2-}$ solution in the absence of **1**, under analogous irradiation conditions] leads to the detection of 12.6 μmol of CO_2 (3.4 times higher with respect to the amount detected in the presence of **1**), suggesting that the primary source of CO_2 is the $Ru(bpy)_3^{2+}$ photosensitizer (12.6 μmol accounts for 0.84 equiv of CO_2 per $Ru(bpy)_3^{2+}$, resulting in an average of 2.8% C atoms from bpy ligands transformed into CO_2). Similarly, 0.44 equiv of CO_2 was detected upon irradiation of $Ru(bpy)_3^{2+}/S_2O_8^{2-}$ in 50 mM phosphate buffer, where the only source of C is the bpy ligands; no CO_2 formation from $Ru(bpy)_3^{2+}$ was observed in the absence of $S_2O_8^{2-}$, showing that decomposition involves the Ru(III)-oxidized form of the photosensitizer.[33] Negligible formation of CO_2 in the presence of Ir precatalysts within the $Ru(bpy)_3^{2+}/S_2O_8^{2-}$ photoactivated system was also noticed by Pandey et al.[30] Thus, as a further benefit, the presence of the Ir precatalyst **1** induces photoprotection of the $Ru(bpy)_3^{2+}$ dye,

DOI: 10.1021/acs.inorgchem.9b02531
Inorg. Chem. XXXX, XXX, XXX−XXX

by rapid reaction with photogenerated $Ru^{III}(bpy)_3^{3+}$ and associated fast regeneration of $Ru^{II}(bpy)_3^{2+}$ (vide infra).

Flash Photolysis and Electron-Transfer Rate from Ir-pyalc Derivatives to Ru(III). In order to gain further insights into the catalyst activation mechanism, we investigated the rate of the primary electron transfer from the Ir-pyalc species to the oxidized form of the photosensitizer $Ru(bpy)_3^{3+}$ (*hole scavenging*)[43−51] along the **1** → **Ir-blue** oxidative dimerization. This can be conveniently revealed by laser flash photolysis, where $Ru(bpy)_3^{3+}$ is photogenerated in a few nanoseconds by laser irradiation (λ_{exc} = 355 nm) of a solution containing $Ru(bpy)_3^{2+}$ and $Na_2S_2O_8$. As discussed above, the formation of $Ru(bpy)_3^{3+}$ is associated with a decrease of the absorbance (*bleaching*) at 450 nm because of depletion of the MLCT transition in the $Ru(bpy)_3^{3+}$-oxidized form. In the presence of the Ir precatalyst **1**, the recovery of the absorbance at 450 nm in a ca. 100 μs time scale (Figure 2, top) is associated with backconversion of Ru(III) to Ru(II) due to electron transfer from **1** (*primary hole scavenging*; eq 4) converting **1** into a one-electron-oxidized intermediate $\mathbf{I_1}$. When the experiment is conducted with different concentrations of **1** (0.25−0.50 mM) under pseudo-first-order conditions ([**1**] ≫ [Ru(III)]), the traces can be fitted with single-exponential functions, providing the observed first-order rate constants of the processes k_{obs} (eq 5). It is then possible to determine a second-order rate constant $k_1 = (1.00 \pm 0.02) \times 10^8\ M^{-1}\ s^{-1}$ for the primary hole scavenging, given by the slope of the plot of k_{obs} values versus the concentration of **1** (Figure S5) according to eq 6.

$$Ru(III) + \mathbf{1} \rightarrow Ru(II) + \mathbf{I_1} \quad (4)$$

$$d[Ru(II)]/dt = -d[Ru(III)]/dt = k_{obs}[Ru(III)] \quad (5)$$

$$k_{obs} = k_1[\mathbf{1}] \quad (6)$$

The value of $k_1 = (1.00 \pm 0.02) \times 10^8\ M^{-1}\ s^{-1}$ is more than 1 order of magnitude lower than the one expected for a diffusion-limited process,[50] suggesting a partial reorganization energy associated with electron transfer. However, k_1 is considerably larger than the bimolecular rate constants of electron transfer to $Ru(bpy)_3^{3+}$ observed for other Ir(III) species bearing a Cp* ligand and a bidentate ligand such as bpy and a dicarbene 1,1-dimethyl-3,3-ethylenediimidazole-2,2-diylidene (di-NHC), for which rate constants for primary hole scavenging are $(5.1 \pm 0.4) \times 10^4$ and $(2.90 \pm 0.01) \times 10^5\ M^{-1}\ s^{-1}$, respectively (Figures S6 and S7 and Table S2). This feature can be associated with the electron-donating nature of the pyalc ligand, providing easier access to the Ir(IV) state, thus highlighting the important role of the chelating ligand to enable facile and fast activation of the Ir(III) precatalyst.

The nature of the $\mathbf{I_1}$ species generated along the primary hole scavenging to Ru(III) can be discussed according to the spectral evolution of the transient signal registered during the time scale of the experiment (Figure 2, middle): in particular, this shows the development of two new broad absorptions centered at ca. 470 and 650 nm along with the disappearance of the Ru(III) species. These spectral features remain persistent within the time window of the experiment (80 ms, inset in Figure 2, middle) and resemble those observed for a mononuclear Ir^{IV}-pyalc derivative,[52] which can, therefore, be postulated as the primary intermediate $\mathbf{I_1}$ formed upon oxidation of **1** with $Ru(bpy)_3^{3+}$ (eq 7). This mononuclear Ir(IV) species $\mathbf{I_1}$ is expected to be the forerunner of a series of

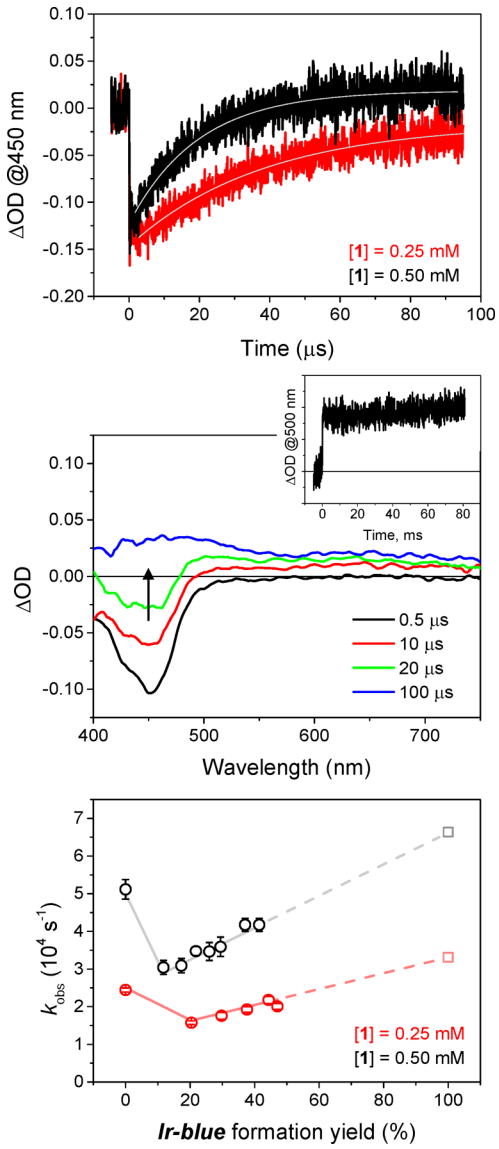

Figure 2. Top: Flash photolysis kinetics showing electron transfer between **1** and $Ru(bpy)_3^{3+}$ (*primary hole scavenging*) monitored by the bleach recovery at 450 nm [excitation at 355 nm, fwhm = 8 ns in 50 mM $Na_2SiF_6/NaHCO_3$ buffer (pH = 5.2) solutions containing 50 μM $Ru(bpy)_3^{2+}$, 5 mM $Na_2S_2O_8$, and 0.25 (red trace) or 0.50 mM (black trace) **1**]. Middle: Transient absorption spectra at different time delays (0.5−100 μs) in the experiment conducted with 0.50 mM **1** and kinetic analysis at 500 nm (inset). Bottom: Plot of the observed rate constants k_{obs} for Ir → Ru(III) electron transfer [given by Ru(II) recovery] versus the **Ir-blue** formation yield starting with 0.25 mM (red dots) or 0.50 mM (black dots) **1**.

intermediates $\mathbf{I}_i$ along evolution of the precatalyst **1** to the **Ir-blue** mixture (eqs 8 and 9).

$$\mathbf{1} \rightarrow \mathbf{I_1} \quad [1e^- \text{ Ir(III) to Ir(IV) oxidation}] \quad (7)$$

$$\mathbf{I_1} \rightarrow \mathbf{I}_i \rightarrow \mathbf{I}_n \quad \text{(further oxidation steps)} \quad (8)$$

$$\mathbf{I}_n \rightarrow \textbf{Ir-blue} \quad (9)$$

In this respect, additional information comes from variation of the k_{obs} values associated with Ir → Ru(III) electron transfer, when monitored at increasing conversion of the precatalyst **1** to **Ir-blue**. The flash photolysis experiments were indeed conducted with solutions initially containing **1**,

DOI: 10.1021/acs.inorgchem.9b02531
Inorg. Chem. XXXX, XXX, XXX−XXX

$Ru(bpy)_3^{2+}$, and $Na_2S_2O_8$ and then irradiated at different times, allowing a progressive increase of the amount of photogenerated **Ir-blue** (this is determined by UV−vis spectroscopy, as previously discussed). Figure 2, bottom, reports the plot of k_{obs} of Ir → Ru(III) electron transfer versus the yield of **Ir-blue** formation, starting from two different concentrations of **1** (0.25 and 0.50 mM; it is worth mentioning that, under these conditions, the formation of **Ir-blue** is slower and takes ca. 1 h because of the lower amount of photogenerated Ru(III) oxidant; see Figure S8); in both cases, the plot shows a segmented profile, with an initial drop of the k_{obs} values (up to ca. 60% of its initial value), followed by a linear increase of k_{obs} above 20% yield of **Ir-blue** conversion, at both 0.25 and 0.50 mM initial concentrations of **1** (Figure 2, bottom). This behavior can be explained by the formation of intermediates along the conversion of **1** into **Ir-blue** (eqs 7 and 8), showing, on average, a slower reactivity toward electron transfer to Ru(III) with respect to both **1** and **Ir-blue**. Indeed, assuming that the diverse intermediates $\mathbf{I}_n$ formed from **1** can perform electron transfer to Ru(III) and thus contribute to the primary hole scavenging event, the observed rate constant k_{obs} can be expressed according to eqs 10 and 11, where $k_{\mathbf{I}_i}$ and $[\mathbf{I}_i]$ are the bimolecular rate constant and the concentration of intermediate $\mathbf{I}_i$, respectively.

$$k_{obs} = k_1[\mathbf{1}] + \sum k_{\mathbf{I}_i}[\mathbf{I}_i] + k_{\textbf{Ir-blue}}[\textbf{Ir-blue}]; \quad i = 1 - n \tag{10}$$

$$k_{\text{I-average}} = \sum k_{\mathbf{I}i}[\mathbf{I}_i]/\sum[\mathbf{I}_i] \tag{11}$$

Simulation of the experimental data with a theoretical model according to eq 10 (solid lines in Figure 2, bottom) provides a weighted-average $k_{\text{I-average}} = (4.80 \pm 0.10) \times 10^7\ M^{-1}\ s^{-1}$ and $k_{\textbf{Ir-blue}} = (2.65 \pm 0.05) \times 10^8\ M^{-1}\ s^{-1}$ (see the Supporting Information for details on the kinetic model). Interestingly, the $k_{\textbf{Ir-blue}}$ value estimated from these data is in fairly good agreement with the value of $k_{\textbf{Ir-blue}}' = (3.00 \pm 0.02) \times 10^8\ M^{-1}\ s^{-1}$, obtained for the **Ir-blue** species generated by chemical oxidation of **1** with $NaIO_4$ (Figure S9). In the case of **Ir-blue**, the hole scavenging is likely related to the oxidation of Ir(IV) centers to Ir(V),[10] which are considered to be the active sites in the oxygen evolution cycle. A pertinent comparison deals with iridium oxide nanoparticles IrO_x, for which a bimolecular rate constant of $k_{IrOx} = 1.3 \times 10^6\ M^{-1}\ s^{-1}$ was observed under similar conditions.[32,34] The higher value observed for **Ir-blue** can likely be associated with the low potential required to access the Ir(V) states, residing close to the thermodynamic value of the O_2/H_2O couple [0.92 V vs NHE at pH = 5.2, with a favorable driving force by 310 mV for oxidation by $Ru(bpy)_3^{3+}$; see the cyclic voltammetries in Figure S10]. As an additional figure-of-merit, $k_{\textbf{Ir-blue}}$ is larger with respect to k_1 registered for precursor **1**, where the redox transition involves the oxidation of Ir(III) to Ir(IV); see the previous discussion. Although this evidence may be affected also by the statistical contribution originating from the presence of two Ir centers in **Ir-blue**, this result is consistent with a more favorable access to higher oxidation states in the dinuclear form, likely ascribable to the donor ability of the μ-oxo ligand and possibly involving proton-coupled electron-transfer processes.

Finally, flash photolysis experiments were properly designed in order to reveal the number of electron-transfer events from **Ir-blue** to $Ru(bpy)_3^{3+}$, occurring in a sufficiently long time scale of ca. 50 ms; this was accomplished by employing substoichiometric **Ir-blue** concentrations with respect to photogenerated Ru(III).[43−51] In this case, the recovery of the absorption at 450 nm accounts for two electron-transfer events in ca. 10 ms [Figure S9; the number of electron transfers is given by the amount of Ru(II) recovered with respect to the amount of **Ir-blue** employed], suggesting the fast formation of an $Ir^{V,V}_2$ derivative. Subsequently, the persistent bleaching between 10 and 50 ms indicates that no further reactions occur in this time frame between Ru(III) and the oxidized **Ir-blue** species. Thus, this observation identifies the $Ir^{V,V}_2$ species as the steady-state intermediate that possibly accumulates before the rate-determining step of the oxygen-evolving cycle (vide infra).

Photocatalytic Oxygen Evolution. We finally explored the oxygen-evolving activity of **Ir-blue** within the $Ru(bpy)_3^{2+}/Na_2S_2O_8$ system and first examined the oxygen evolution profile upon irradiation with white light by employing 50 μM **1**, 1 mM $Ru(bpy)_3^{2+}$, and 5 mM $Na_2S_2O_8$ in 15 mL of 50 mM $Na_2SiF_6/NaHCO_3$ aqueous buffer, pH = 5.2, using an experimental setup previously reported.[50] In these conditions (Figure S11 and entry 1 in Table 1), oxygen evolution is observed after a lag time of ca. 2−3 min upon irradiation. This is likely related to the photogeneration and accumulation of $Ru(bpy)_3^{3+}$ and to transformation of the precatalyst **1** into the

Table 1. Parameters for the Light-Driven Water Oxidation Reaction with the $Ru(bpy)_3^{2+}/S_2O_8^{2-}$ System in the Presence of the Precatalyst 1[a]

entry	light source (photon flux; einstein s^{-1})	$R_0(O_2) \times 10^3$,[b] μmol s^{-1} (TOF × 10^3, s^{-1})	μmol of O_2[c] (TON)	yield (%) on $Na_2S_2O_8$
1	white light (not measured)	3.2 ± 0.2 (4.3 ± 0.3)	16.5 ± 0.5 (21.9 ± 0.6)	44 ± 1
2	blue LED (4.42×10^{-9})	1.40 ± 0.05 (1.89 ± 0.07)	16.0 ± 0.5 (21.3 ± 0.6)	43 ± 1
3	blue LED (1.77×10^{-8})	3.9 ± 0.3 (5.2 ± 0.4)	16.8 ± 0.8 (22.4 ± 1.1)	45 ± 2
4	blue LED (3.54×10^{-8})	6.4 ± 0.4 (8.5 ± 0.5)	24.4 ± 1.1 (32.0 ± 1.5)	65 ± 3
5	blue LED (5.30×10^{-8})	7.5 ± 0.5 (10.0 ± 0.7)	20.0 ± 1.2 (26.7 ± 1.6)	53 ± 3
6	blue LED (1.06×10^{-7})	8.2 ± 0.4 (10.9 ± 0.5)	15.2 ± 1.4 (20.3 ± 1.9)	40 ± 3
7	blue LED (2.12×10^{-7})	9.7 ± 0.3 (12.9 ± 0.5)	14.3 ± 1.9 (19.0 ± 2.5)	38 ± 5

[a]Reaction conditions: 15 mL of 50 mM $Na_2SiF_6/NaHCO_3$ buffer, pH = 5.2; $[Ru(bpy)_3^{2+}]$ = 1 mM; $[Na_2S_2O_8]$ = 5 mM; [**1**] = 50 μM (loaded from a 2.5 mM solution prepared in the same buffer). Irradiation in entry 1 was performed with white light (3.8 mW cm^{-2}). Irradiation in entries 2−7 was performed with a series of six monochromatic LEDs emitting at 450 nm (4.42×10^{-9}−2.12×10^{-7} einstein s^{-1}). [b]$R_0(O_2)$ values were determined by a linear fitting of the experimental traces, from 10 to 20 min after light was turned on. In the case of the kinetic trace conducted with photon flux = 4.42×10^{-9} einstein s^{-1} (black trace in Figure 3, top, and entry 2 in Table 1), the rate $R_0(O_2)$ was determined by a linear fitting between 120 and 180 min: the extended lag time of oxygen formation under these conditions is ascribable to slow photogeneration and accumulation of the active **Ir-blue**. [c]The micromoles of oxygen were determined when the oxygen evolution kinetics reached the plateau; the maximum oxygen produced is given by 0.5 × μmol($Na_2S_2O_8$) and equal to 37.5 μmol in the conditions adopted (although this limit can be an overestimation because some of oxidizing equivalents are needed to generate the **Ir-blue** catalyst from **1**): as a consequence, the maximum TON per Ir center is equal to 50.

DOI: 10.1021/acs.inorgchem.9b02531
Inorg. Chem. XXXX, XXX, XXX−XXX

active **Ir-blue** WOC (slow diffusion of gaseous oxygen from the solution to the headspace of the reactor could also contribute to some extent). After this initial delay, oxygen evolution is observed with a maximum rate of $(3.2 \pm 0.2) \times 10^{-3}$ μmol of O_2 s^{-1} [TOF per Ir center, $(4.3 \pm 0.3) \times 10^{-3}$ s^{-1}] and proceeds for ca. 180 min, until reaching a plateau of 16.5 ± 0.5 μmol of O_2 evolved, corresponding to $44 \pm 1\%$ persulfate conversion and to 21.9 ± 0.6 TON per Ir center. The reason for the ceased activity can be ascribed to a combination of persulfate consumption and photosensitizer partial decomposition,[35] as demonstrated by restored photo-induced oxygen production by recharging the solution with persulfate (Figure S11) and by the UV−vis traces of the spent reaction solution [showing a partial bleaching of the $Ru(bpy)_3^{2+}$ MLCT absorption; Figure S12]. The UV−vis traces confirm also the persistence of the **Ir-blue** species in the spent mixture, as demonstrated by the fingerprint absorption at 590 nm (see the differential absorption spectrum in Figure S12).

Water was confirmed to be the origin of evolved oxygen by conducting an experiment in 25% ^{18}O-enriched water and analyzing the gas phase by means of gas chromatography coupled to mass spectrometry, which revealed an experimental isotopic pattern for oxygen that matches the one simulated by taking into account the isotopic composition of water (Figure S13).

In the $Ru(bpy)_3^{2+}/S_2O_8^{2-}$/**Ir-blue** system, light should actually be considered to be a reactant, and the overall performance in terms of the initial rate, quantum yield, and total amount of oxygen production may depend by all steps 1−8 in Scheme S1 or by a combination of them.[26,48,53] Therefore, we examined the oxygen evolution profiles in the conditions above by irradiating with blue light-emitting diodes (LEDs) [450 nm; full width at half-maximum (fwhm) = 10 nm] and solely tuning the light intensity in the range of 4.42×10^{-9}−2.12×10^{-7} einstein s^{-1}. Figure 3 (top panel) shows the oxygen evolution profiles obtained, while the oxygen evolution rate, total amount of oxygen produced, and $Na_2S_2O_8$ conversion are reported in Table 1.

Interestingly, both the total oxygen production (and the correlated value of TON, given per Ir center) and maximum oxygen evolution rate (and the correlated value of TOF, given per Ir center) depend on the light intensity (Figure 3 and Table 1, entries 2−7). We exploited the maximum oxygen evolution rate and the derived value of the TOF calculated per Ir center, as a key marker of the performance of the system (Figure 3, bottom). These are determined after the initial lag time, between 10 and 20 min after irradiation, where the oxygen evolution process shows a linear kinetic regime [in the case of the kinetic trace conducted at "low light intensity" with photon flux = 4.42×10^{-9} einstein s^{-1} (black trace in Figure 3, top), the rate $R_0(O_2)$ was determined by a linear fitting between 120 and 180 min]. The dependence of the TOF on the light intensity shows a clear two-regime behavior (Figure 3, bottom, black dots).

In a first segment with photon flux below 5.3×10^{-8} einstein s^{-1}, the TOF shows a direct dependence on the light intensity; this is indicative of light being a limiting reagent, with photogeneration of $Ru(bpy)_3^{3+}$ as the rate-determining step of the overall photocatalytic cycle (steps 1−3 in Scheme S1).[26] Under these conditions, at a photon flux = 4.42×10^{-8} einstein s^{-1}, an oxygen evolution rate of $(1.40 \pm 0.05) \times 10^{-9}$ mol of O_2 s^{-1} was observed, corresponding to an impressive quantum yield for oxygen evolution $\phi(O_2) = 0.32 \pm 0.01$, determined by the ratio of $R_0(O_2)$ and the absorbed photon flux (Figure 3, bottom, red dots); a value $\phi(O_2) = 0.11$ was previously obtained by Corbucci et al. with $[Cp^*Ir(H_2O)_3]^{2+}$ and $[Cp^*_2IrCl_2L_2]$ (L = *N*-dimethylimidazolin-2-ylidene).[28] It should be highlighted that the $\phi(O_2) = 0.32 \pm 0.01$ value corresponds to a quantum efficiency[48] for oxygen evolution of $64 \pm 2\%$ because a theoretical maximum quantum yield $\phi(O_2) = 0.50$ is expected with the $Ru(bpy)_3^{2+}/S_2O_8^{2-}$ cycle [indeed, the production of one oxygen molecule theoretically requires the absorption of two photons, necessary for the generation of 4 equiv of $Ru(bpy)_3^{3+}$, Scheme S1].[48]

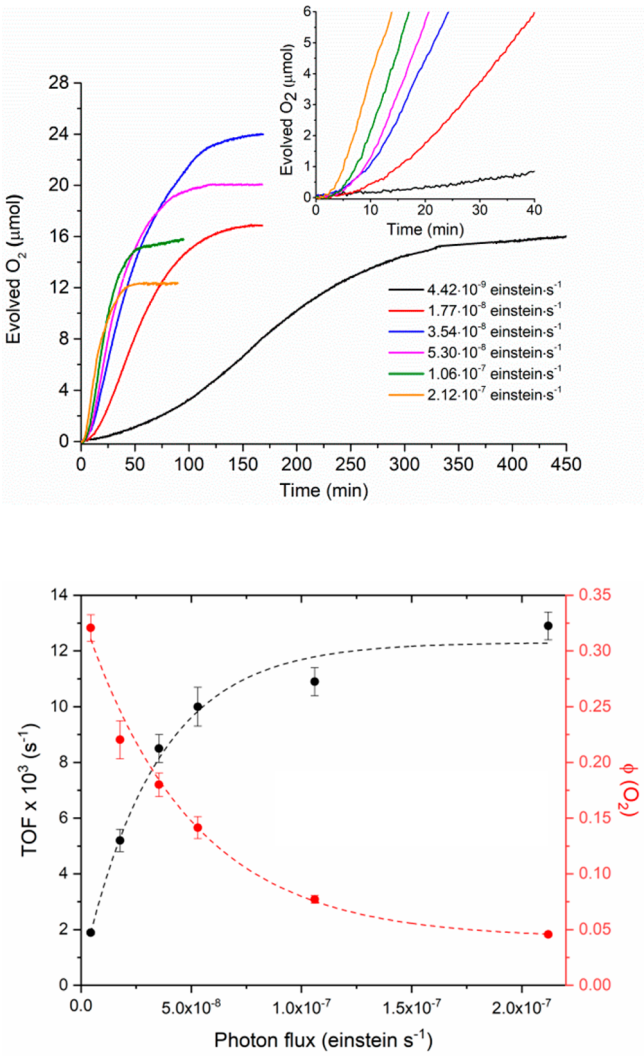

Figure 3. Top: Oxygen evolution kinetics with the precatalyst **1** at different light intensities (4.42×10^{-9}−2.12×10^{-7} einstein s^{-1} with monochromatic LEDs emitting at 450 nm and fwhm = 10 nm). The inset shows a magnification of the traces in the initial time frame, where oxygen evolution is observed after a lag time of 2−10 min upon irradiation, depending on the irradiation conditions (a longer lag time is observed with low-intensity irradiation). Reaction conditions: 15 mL of 50 mM $Na_2SiF_6/NaHCO_3$ buffer, pH = 5.2; $[Ru(bpy)_3^{2+}]$ = 1 mM; $[Na_2S_2O_8]$ = 5 mM; [**1**] = 50 μM (introduced from a freshly prepared 2.5 mM solution in the same buffer; superimposable traces were obtained using aged stock solutions of **1** up to 24 h). Bottom: Maximum TOF ($\times 10^3$) per Ir center and quantum yield for oxygen evolution $\phi(O_2)$ versus photon flux. The dashed lines were added for visualization and do not come from fittings.

DOI: 10.1021/acs.inorgchem.9b02531
Inorg. Chem. XXXX, XXX, XXX−XXX

Above the aforementioned light-intensity threshold of 5.3×10^{-8} einstein s^{-1}, the TOF values are almost unchanged, reaching values comprised between 1.1 and 1.3×10^{-2} s^{-1} (Figure 3, bottom). The saturation regime of the TOF under the conditions of "high light intensity" is consistent with a dark, chemical step being rate-determining[49] and involving the $Ir^{V,V}_2$ steady-state intermediate as previously envisaged by flash photolysis evidence (see the previous discussion and Figure S9). Because further oxidation of the Ir centers seems unlikely, this rate-determining step can be ascribed to formation of the O−O bond from such an oxidized form of **Ir-blue** (step 8 in Scheme S1). This is consistent with a previous hypothesis that envisaged an $Ir^{V,V}_2$ intermediate as the one responsible for O−O bond formation when the Ir WOC was chemisorbed onto metal oxide surfaces.[10] Besides the nature of this chemical rate-determining step, the leveling off of the oxygen-evolving rates implies that an increase of the light intensity above the threshold of 5.3×10^{-8} einstein s^{-1} is not effective in driving catalysis and can promote undesired, competitive reactions. Indeed, under this regime, the quantum yield of oxygen production drops progressively, down to the 0.05 value observed at photon flux 2.12×10^{-7} einstein s^{-1}.

This observation is also consistent with the plot of the total oxygen produced versus photon flux (Figure S14), showing a profile with a maximum reached at 3.54×10^{-8} einstein s^{-1} (see the blue trace in Figure 3, top, reaching 24 μmol of O_2 and corresponding to 32 TON per Ir center and to 65% conversion of $Na_2S_2O_8$). While an increase of the total oxygen production with increasing light intensity could be expected because of the higher amount of photogenerated $Ru(bpy)_3^{3+}$ oxidant feeding the Ir species, depletion of the total oxygen production at high irradiation intensity may be ascribed to favored routes of photosensitizer decomposition.[26,35,36,48] These unproductive routes might indeed become more pronounced when the catalysis rate cannot compensate for a faster accumulation of photogenerated $Ru(bpy)_3^{3+}$ species (see above discussion). The adequate matching of light and chemistry rates seems, therefore, an important parameter to be considered, in particular when mechanistically complex transformations are associated with the photoactivated step.

Finally, we point out some features and limitations of the photoactivated $Ru(bpy)_3^{2+}/S_2O_8^{2-}$ cycle when combined with a WOC. Because the maximum production of oxygen depends on the amount of persulfate used (maximum moles of produced oxygen = 0.5 × moles of persulfate employed), the maximum TON of the catalyst depends on the $S_2O_8^{2-}$/catalyst ratio (TON_{MAX} = 0.5 × moles of persulfate/moles of WOC). These values are, however, upper limits because competitive oxidation processes may occur, such as $Ru(bpy)_3^{2+}$ photosensitizer degradation.[35−37] Other factors that may impact the efficiency of the cycle are a pH decrease because water oxidation is accompanied by the release of four protons, quenching of the photosensitizer by produced oxygen, involvement of the buffer in assisting proton-coupled electron transfer,[51] and formation of ion pairs.[43,46,49,50] As such, with respect to electrochemical methods,[10a] the photochemical $Ru(bpy)_3^{2+}/S_2O_8^{2-}$ system is not ideal for testing the durability of a WOC in terms of high TON, which can be reached only when using $[WOC] \ll [S_2O_8^{2-}]$.[50] Conversely, the performance of a $Ru(bpy)_3^{2+}/S_2O_8^{2-}$/WOC system should be considered to be a property of the whole cycle rather than of the sole catalyst, and the most indicative key performance indicator in this sense is the quantum yield, or the derived value of the quantum efficiency.[48,50] We point out that the investigation of photochemical cycles of this type can be relevant for the design and development of photoelectrochemical systems, where the oxidizing equivalents delivered to the catalyst are provided by a photogenerated oxidant, typically a photooxidized sensitizer.[50] In this sense, the photochemical cycles may be exploited to obtain complementary mechanistic information with respect to electrochemical tools, related to the catalyst/photosensitizer association, electron-transfer dynamics, and characterization of competent intermediates.

■ CONCLUSIONS

We have reported here for the first time the fast photogeneration of the dinuclear **Ir-blue** WOC from the Ir(III) mononuclear precursor **1** (up to 15 min; $\phi_{\text{Ir-blue}}$ of up to 0.10) through the $Ru(bpy)_3^{2+}/S_2O_8^{2-}$ cycle. Water oxidation catalysis under visible light by **Ir-blue** is also promoted by this photochemical system, reaching $\phi(O_2)$ of up to 0.32 ± 0.01 (quantum efficiency of 64 ± 2%) and likely involving a fast-generated $Ir^{V,V}_2$ steady-state intermediate operating in the rate-determining O−O bond formation regime.

Investigation of the system by flash photolysis allows determination of the electron-transfer rate constant from Ir(pyalc) species to $Ru^{III}(bpy)_3^{3+}$ ($k \sim 10^8$ M^{-1} s^{-1}), several orders of magnitude higher with respect to other Ir species and likely associated with the electron-donating nature of the pyalc ligand that favors access to highly oxidized Ir states.

Characterization and kinetic evidence of intermediates along **1**-to-**Ir-blue** conversion come from a combination of transient absorption spectroscopy [suggesting an Ir(IV) mononuclear species formed from **1** upon the first oxidizing equivalent] and the segmented trend of the observed rate constants for Ir → Ru(III) electron transfer.

Finally, the light dependence of oxygen evolution kinetics highlights the presence of light or chemistry governing regimes in photocatalysis, where an efficient exploitation of the light source needs a proper matching with the light "reactant". This concept should be applied also in the case of photoelectrodes in order to optimize light absorption and charge separation while avoiding undesired competitive reactions in view of improved efficiency and durability of photoactive devices.

■ ASSOCIATED CONTENT

Supporting Information

The Supporting Information is available free of charge at https://pubs.acs.org/doi/10.1021/acs.inorgchem.9b02531.

Synthetic procedures, analytical methods, electrochemical data, photophysical spectra, and kinetic traces (PDF)

■ AUTHOR INFORMATION

Corresponding Authors

*Email: mirco.natali@unife.it (M.N.).
*Email: andrea.sartorel@unipd.it (A.S.).

ORCID

Cristina Tubaro: 0000-0001-7724-735X
Mirco Natali: 0000-0002-6638-978X
Andrea Sartorel: 0000-0002-4310-3507
Gary W. Brudvig: 0000-0002-7040-1892
Marcella Bonchio: 0000-0002-7445-0296

DOI: 10.1021/acs.inorgchem.9b02531
Inorg. Chem. XXXX, XXX, XXX−XXX

Author Contributions

The manuscript was written through contributions of all authors. All authors have given approval to the final version of the manuscript.

Notes

The authors declare no competing financial interest.

■ ACKNOWLEDGMENTS

A.S. thanks the Department of Chemical Sciences at the University of Padova and Fondazione Cassa di Risparmio di Padova e Rovigo for funding (Project PHOETRY, P-DiSC #10BIRD2018-UNIPD, and Project SYNERGY, Ricerca Scientifica di Eccellenza 2018). G.W.B. is thankful for funding from the U.S. Department of Energy, Office of Science, Office of Basic Energy Sciences, under Award DE-SC0001059 as part of the Center for Light Energy Activated Redox Processes (LEAP), Energy Frontier Research Center.

■ REFERENCES

(1) Zhang, B.; Sun, L. Artificial Photosynthesis: Opportunities and Challenges of Molecular Catalysts. *Chem. Soc. Rev.* **2019**, *48* (7), 2216−2264.

(2) El-Khouly, M. E.; El-Mohsnawy, E.; Fukuzumi, S. Solar Energy Conversion: From Natural to Artificial Photosynthesis. *J. Photochem. Photobiol., C* **2017**, *31*, 36−83.

(3) Berardi, S.; Drouet, S.; Francàs, L.; Gimbert-Suriñach, C.; Guttentag, M.; Richmond, C.; Stoll, T.; Llobet, A. Molecular Artificial Photosynthesis. *Chem. Soc. Rev.* **2014**, *43* (22), 7501−7519.

(4) McDaniel, N. D.; Coughlin, F. J.; Tinker, L. L.; Bernhard, S. Cyclometalated Iridium(III) Aquo Complexes: Efficient and Tunable Catalysts for the Homogeneous Oxidation of Water. *J. Am. Chem. Soc.* **2008**, *130* (1), 210−217.

(5) Macchioni, A. The Middle-Earth between Homogeneous and Heterogeneous Catalysis in Water Oxidation with Iridium. *Eur. J. Inorg. Chem.* **2019**, *2019*, 7−17.

(6) Blakemore, J. D.; Crabtree, R. H.; Brudvig, G. W. Molecular Catalysts for Water Oxidation. *Chem. Rev.* **2015**, *115* (23), 12974−13005.

(7) Woods, J. A.; Lalrempuia, R.; Petronilho, A.; McDaniel, N. D.; Müller-Bunz, H.; Albrecht, M.; Bernhard, S. Carbene Iridium Complexes for Efficient Water Oxidation: Scope and Mechanistic Insights. *Energy Environ. Sci.* **2014**, *7* (7), 2316−2328.

(8) (a) Lalrempuia, R.; McDaniel, N. D.; Müller-Bunz, H.; Bernhard, S.; Albrecht, M. Water Oxidation Catalyzed by Strong Carbene-Type Donor-Ligand Complexes of Iridium. *Angew. Chem., Int. Ed.* **2010**, *49* (50), 9765−9768. (b) Menendez Rodriguez, G.; Bucci, A.; Hutchinson, R.; Bellachioma, G.; Zuccaccia, C.; Giovagnoli, S.; Idriss, H.; Macchioni, A. Extremely Active, Tunable, and pH-Responsive Iridium Water Oxidation Catalysts. *ACS Energy Lett.* **2017**, *2*, 105−110.

(9) Michaelos, T. K.; Shopov, D. Y.; Sinha, S. B.; Sharninghausen, L. S.; Fisher, K. J.; Lant, H. M. C.; Crabtree, R. H.; Brudvig, G. W. A Pyridine Alkoxide Chelate Ligand That Promotes Both Unusually High Oxidation States and Water-Oxidation Catalysis. *Acc. Chem. Res.* **2017**, *50* (4), 952−959.

(10) (a) Sheehan, S. W.; Thomsen, J. M.; Hintermair, U.; Crabtree, R. H.; Brudvig, G. W.; Schmuttenmaer, C. A.. A Molecular Catalyst for Water Oxidation That Binds to Metal Oxide Surfaces. *Nat. Commun.* **2015**, *6*, article number 6469. DOI: 10.1038/ncomms7469 (b) Menendez Rodriguez, G.; Gatto, G.; Zuccaccia, C.; Macchioni, A. Benchmarking Water Oxidation Catalysts Based on Iridium Complexes: Clues and Doubts on the Nature of Active Species. *ChemSusChem* **2017**, *10*, 4503−4509.

(11) Thomsen, J. M.; Sheehan, S. W.; Hashmi, S. M.; Campos, J.; Hintermair, U.; Crabtree, R. H.; Brudvig, G. W. Electrochemical Activation of Cp* Iridium Complexes for Electrode-Driven Water-Oxidation Catalysis. *J. Am. Chem. Soc.* **2014**, *136* (39), 13826−13834.

(12) Detz, R. J.; Sakai, K.; Spiccia, L.; Brudvig, G. W.; Sun, L.; Reek, J. N. H. Towards a Bioinspired-Systems Approach for Solar Fuel Devices. *ChemPlusChem* **2016**, *81* (10), 1024−1027.

(13) Koelewijn, J. M.; Lutz, M.; Detz, R. J.; Reek, J. N. H. Anode Preparation Strategies for the Electrocatalytic Oxidation of Water Based on Strong Interactions between Multiwalled Carbon Nanotubes and Cationic Acetylammonium Pyrene Moieties in Aqueous Solutions. *ChemPlusChem* **2016**, *81* (10), 1098−1106.

(14) Poddutoori, P. K.; Thomsen, J. M.; Milot, R. L.; Sheehan, S. W.; Negre, C. F. A.; Garapati, V. K. R.; Schmuttenmaer, C. A.; Batista, V. S.; Brudvig, G. W.; Van Der Est, A. Interfacial Electron Transfer in Photoanodes Based on Phosphorus(V) Porphyrin Sensitizers Co-Deposited on SnO_2 with the Ir(III)Cp* Water Oxidation Precatalyst. *J. Mater. Chem. A* **2015**, *3* (7), 3868−3879.

(15) Kamire, R. J.; Materna, K. L.; Hoffeditz, W. L.; Phelan, B. T.; Thomsen, J. M.; Farha, O. K.; Hupp, J. T.; Brudvig, G. W.; Wasielewski, M. R. Photodriven Oxidation of Surface-Bound Iridium-Based Molecular Water-Oxidation Catalysts on Perylene-3,4-Dicarboximide-Sensitized TiO_2 Electrodes Protected by an Al_2O_3 Layer. *J. Phys. Chem. C* **2017**, *121* (7), 3752−3764.

(16) Materna, K. L.; Jiang, J.; Regan, K. P.; Schmuttenmaer, C. A.; Crabtree, R. H.; Brudvig, G. W. Optimization of Photoanodes for Photocatalytic Water Oxidation by Combining a Heterogenized Iridium Water-Oxidation Catalyst with a High-Potential Porphyrin Photosensitizer. *ChemSusChem* **2017**, *10* (22), 4526−4534.

(17) Sinha, S. B.; Shopov, D. Y.; Sharninghausen, L. S.; Stein, C. J.; Mercado, B. Q.; Balcells, D.; Pedersen, T. B.; Reiher, M.; Brudvig, G. W.; Crabtree, R. H. Redox Activity of Oxo-Bridged Iridium Dimers in an N, O-Donor Environment: Characterization of Remarkably Stable Ir(IV,V) Complexes. *J. Am. Chem. Soc.* **2017**, *139* (28), 9672−9683.

(18) Sharninghausen, L. S.; Sinha, S. B.; Shopov, D. Y.; Mercado, B. Q.; Balcells, D.; Brudvig, G. W.; Crabtree, R. H. Synthesis and Characterization of Iridium(V) Coordination Complexes With an N, O-Donor Organic Ligand. *Angew. Chem., Int. Ed.* **2017**, *56* (42), 13047−13051.

(19) Sharninghausen, L. S.; Sinha, S. B.; Shopov, D. Y.; Choi, B.; Mercado, B. Q.; Roy, X.; Balcells, D.; Brudvig, G. W.; Crabtree, R. H. High Oxidation State Iridium Mono-μ-Oxo Dimers Related to Water Oxidation Catalysis. *J. Am. Chem. Soc.* **2016**, *138* (49), 15917−15926.

(20) Hintermair, U.; Hashmi, S. M.; Elimelech, M.; Crabtree, R. H. Particle Formation during Oxidation Catalysis with Cp* Iridium Complexes. *J. Am. Chem. Soc.* **2012**, *134* (23), 9785−9795.

(21) Hintermair, U.; Sheehan, S. W.; Parent, A. R.; Ess, D. H.; Richens, D. T.; Vaccaro, P. H.; Brudvig, G. W.; Crabtree, R. H. Precursor Transformation during Molecular Oxidation Catalysis with Organometallic Iridium Complexes. *J. Am. Chem. Soc.* **2013**, *135* (29), 10837−10851.

(22) Parent, A. R.; Crabtree, R. H.; Brudvig, G. W. Comparison of Primary Oxidants for Water-Oxidation Catalysis. *Chem. Soc. Rev.* **2013**, *42* (6), 2247−2252.

(23) Zhao, Y.; Yang, K. R.; Wang, Z.; Yan, X.; Cao, S.; Ye, Y.; Dong, Q.; Zhang, X.; Thorne, J. E.; Jin, L.; et al. Stable Iridium Dinuclear Heterogeneous Catalysts Supported on Metal-Oxide Substrate for Solar Water Oxidation. *Proc. Natl. Acad. Sci. U. S. A.* **2018**, *115* (12), 2902−2907.

(24) Bonchio, M.; Syrgiannis, Z.; Burian, M.; Marino, N.; Pizzolato, E.; Dirian, K.; Rigodanza, F.; Volpato, G. A.; La Ganga, G.; Demitri, N.; et al. Hierarchical Organization of PeryleneBisimides and Polyoxometalates for Photo-Assisted Water Oxidation. *Nat. Chem.* **2019**, *11* (2), 146−153.

(25) Genoni, A.; Chirdon, D. N.; Boniolo, M.; Sartorel, A.; Bernhard, S.; Bonchio, M. Tuning Iridium Photocatalysts and Light Irradiation for Enhanced CO_2 Reduction. *ACS Catal.* **2017**, *7* (1), 154−160.

(26) Limburg, B.; Bouwman, E.; Bonnet, S. Rate and Stability of Photocatalytic Water Oxidation Using $[Ru(Bpy)_3]^{2+}$ as Photosensitizer. *ACS Catal.* **2016**, *6* (8), 5273−5284.

(27) Volpe, A.; Sartorel, A.; Tubaro, C.; Meneghini, L.; Di Valentin, M.; Graiff, C.; Bonchio, M. N-Heterocyclic Dicarbene Iridium(III)

DOI: 10.1021/acs.inorgchem.9b02531
Inorg. Chem. XXXX, XXX, XXX−XXX

Catalysts Enabling Water Oxidation under Visible Light Irradiation. *Eur. J. Inorg. Chem.* **2014**, *2014* (4), 665−675.
(28) Corbucci, I.; Ellingwood, K.; Fagiolari, L.; Zuccaccia, C.; Elisei, F.; Gentili, P. L.; Macchioni, A. Photocatalytic Water Oxidation Mediated by Iridium Complexes. *Catal. Today* **2017**, *290*, 10−18.
(29) Chen, H. C.; Hetterscheid, D. G. H.; Williams, R. M.; Van Der Vlugt, J. I.; Reek, J. N. H.; Brouwer, A. M. Platinum(II)-Porphyrin as a Sensitizer for Visible-Light Driven Water Oxidation in Neutral Phosphate Buffer. *Energy Environ. Sci.* **2015**, *8* (3), 975−982.
(30) Mukhopadhyay, S.; Singh, R. S.; Biswas, A.; Pandey, D. S. Photochemical Water Oxidation by Cyclometalated Iridium(III) Complexes: A Mechanistic Insight. *Chem. Commun.* **2016**, *52* (19), 3840−3843.
(31) Hara, M.; Waraksa, C. C.; Lean, J. T.; Lewis, B. A.; Mallouk, T. E. Photocatalytic Water Oxidation in a Buffered Tris(2,2'-Bipyridyl)-Ruthenium Complex-Colloidal IrO_2 System. *J. Phys. Chem. A* **2000**, *104* (22), 5275−5280.
(32) Morris, N. D.; Suzuki, M.; Mallouk, T. E. Kinetics of Electron Transfer and Oxygen Evolution in the Reaction of $Ru(Bpy)_3^{3+}$ with Colloidal Iridium Oxide. *J. Phys. Chem. A* **2004**, *108* (42), 9115−9119.
(33) Hoertz, P. G.; Kim, Y. Il; Youngblood, W. J.; Mallouk, T. E. Bidentate Dicarboxylate Capping Groups and Photosensitizers Control the Size of IrO_2 Nanoparticle Catalysts for Water Oxidation. *J. Phys. Chem. B* **2007**, *111*, 6845−6856.
(34) Gust, D.; Youngblood, W. J.; Kobayashi, Y.; Moore, A. L.; Moore, T. A.; Hoertz, P. G.; Hernandez-Pagan, E. A.; Mallouk, T. E.; Lee, S.-H. A. Photoassisted Overall Water Splitting in a Visible Light-Absorbing Dye-Sensitized Photoelectrochemical Cell. *J. Am. Chem. Soc.* **2009**, *131* (3), 926−927.
(35) Ghosh, P. K.; Brunschwig, B. S.; Chou, M.; Creutz, C.; Sutin, N. Thermal and Light-Induced Reduction of $Ru(Bpy)_3^{3+}$ in Aqueous Solution. *J. Am. Chem. Soc.* **1984**, *106* (17), 4772−4783.
(36) Lin, C. T.; Bottcher, W.; Chou, M.; Creutz, C.; Sutin, N. Mechanism of the Quenching of the Emission of Substituted Polypyridineruthenium(II) Complexes by Iron(III), Chromium(III), and Europium(III) Ions. *J. Am. Chem. Soc.* **1976**, *98*, 6536−6544.
(37) Lewandowska-Andralojc, A.; Polyansky, D. E. Mechanism of the Quenching of the Tris(Bipyridine)Ruthenium(II) Emission by Persulfate: Implications for Photoinduced Oxidation Reactions. *J. Phys. Chem. A* **2013**, *117* (40), 10311−10319.
(38) White, H. S.; Becker, W. G.; Bard, A. J. Photochemistry of the Tris(2,2'-Bipyridine)Ruthenium(II)-Peroxydisulfate System in Aqueous and Mixed Acetonitrile-Water Solutions. Evidence for a Long-Lived Photoexcited Ion Pair. *J. Phys. Chem.* **1984**, *88* (9), 1840−1846.
(39) Bolletta, F.; Juris, A.; Maestri, M.; Sandrini, D. Quantum Yield of Formation of the Lowest Excited State of $Ru(Bpy)_3^{2+}$ and $Ru(Phen)_3^{2+}$. *Inorg. Chim. Acta* **1980**, *44* (C), L175.
(40) Savini, A.; Belanzoni, P.; Bellachioma, G.; Zuccaccia, C.; Zuccaccia, D.; Macchioni, A. Activity and Degradation Pathways of Pentamethyl-Cyclopentadienyl-Iridium Catalysts for Water Oxidation. *Green Chem.* **2011**, *13* (12), 3360−3374.
(41) Zuccaccia, C.; Bellachioma, G.; Bolaño, S.; Rocchigiani, L.; Savini, A.; Macchioni, A. An NMR Study of the Oxidative Degradation of Cp*Ir Catalysts for Water Oxidation: Evidence for a Preliminary Attack on the Quaternary Carbon Atom of the -C-CH_3 Moiety. *Eur. J. Inorg. Chem.* **2012**, *2012* (9), 1462−1468.
(42) Zuccaccia, C.; Bellachioma, G.; Bortolini, O.; Bucci, A.; Savini, A.; Macchioni, A. Transformation of a Cp*-Iridium(III) Precatalyst for Water Oxidation When Exposed to Oxidative Stress. *Chem. - Eur. J.* **2014**, *20* (12), 3446−3456.
(43) Natali, M.; Bazzan, I.; Goberna-Ferrón, S.; Al-Oweini, R.; Ibrahim, M.; Bassil, B. S.; Dau, H.; Scandola, F.; Galán-Mascarós, J. R.; Kortz, U.; et al. Photo-Assisted Water Oxidation by High-Nuclearity Cobalt-Oxo Cores: Tracing the Catalyst Fate during Oxygen Evolution Turnover. *Green Chem.* **2017**, *19* (10), 2416−2426.
(44) Natali, M.; Berardi, S.; Sartorel, A.; Bonchio, M.; Campagna, S.; Scandola, F. Is $[Co_4(H_2O)_2(\alpha\text{-}PW_9O_{34})_2]^{10-}$ a Genuine Molecular Catalyst in Photochemical Water Oxidation? Answers from Time-Resolved Hole Scavenging Experiments. *Chem. Commun.* **2012**, *48*, 8808−8810.
(45) Berardi, S.; La Ganga, G.; Natali, M.; Bazzan, I.; Puntoriero, F.; Sartorel, A.; Scandola, F.; Campagna, S.; Bonchio, M. Photocatalytic Water Oxidation: Tuning Light-Induced Electron Transfer by Molecular Co_4O_4 Cores. *J. Am. Chem. Soc.* **2012**, *134* (27), 11104.
(46) Natali, M.; Orlandi, M.; Berardi, S.; Campagna, S.; Bonchio, M.; Sartorel, A.; Scandola, F. Photoinduced Water Oxidation by a Tetraruthenium Polyoxometalate Catalyst: Ion-Pairing and Primary Processes with $Ru(Bpy)_3^{2+}$ Photosensitizer. *Inorg. Chem.* **2012**, *51* (13), 7324−7331.
(47) Al-Oweini, R.; Sartorel, A.; Bassil, B. S.; Natali, M.; Berardi, S.; Scandola, F.; Kortz, U.; Bonchio, M. Photocatalytic Water Oxidation by a Mixed-Valent $Mn^{III}_3Mn^{IV}O_3$ Manganese Oxo Core That Mimics the Natural Oxygen-Evolving Center. *Angew. Chem., Int. Ed.* **2014**, *53* (42), 11182−11185.
(48) Sartorel, A.; Bonchio, M.; Campagna, S.; Scandola, F. Tetrametallic Molecular Catalysts for Photochemical Water Oxidation. *Chem. Soc. Rev.* **2013**, *42* (6), 2262−2280.
(49) Bazzan, I.; Volpe, A.; Dolbecq, A.; Natali, M.; Sartorel, A.; Mialane, P.; Bonchio, M. Cobalt Based Water Oxidation Catalysis with Photogenerated $Ru(Bpy)_3^{3+}$: Different Kinetics and Competent Species Starting from a Molecular Polyoxometalate and Metal Oxide Nanoparticles Capped with a Bisphosphonate Alendronate Pendant. *Catal. Today* **2017**, *290*, 39−50.
(50) Natali, M.; Nastasi, F.; Puntoriero, F.; Sartorel, A. Mechanistic Insights into Light-Activated Catalysis for Water Oxidation. *Eur. J. Inorg. Chem.* **2019**, *2019*, 2027−2039.
(51) Volpato, G. A.; Bonetto, A.; Marcomini, A.; Mialane, P.; Bonchio, M.; Natali, M.; Sartorel, A. Proton Coupled Electron Transfer from Co_3O_4 Nanoparticles to Photogenerated $Ru(Bpy)_3^{3+}$: Base Catalysis and Buffer Effect. *Sustain. Energy Fuels* **2018**, *2*, 1951−1956.
(52) Shopov, D. Y.; Rudshteyn, B.; Campos, J.; Vinyard, D. J.; Batista, V. S.; Brudvig, G. W.; Crabtree, R. H. A Full Set of Iridium(IV) Pyridine-Alkoxide Stereoisomers: Highly Geometry-Dependent Redox Properties. *Chem. Sci.* **2017**, *8* (2), 1642−1652.
(53) Francàs, L.; Matheu, R.; Pastor, E.; Reynal, A.; Berardi, S.; Sala, X.; Llobet, A.; Durrant, J. R. Kinetic Analysis of an Efficient Molecular Light-Driven Water Oxidation System. *ACS Catal.* **2017**, *7* (8), 5142−5150.

DOI: 10.1021/acs.inorgchem.9b02531
Inorg. Chem. XXXX, XXX, XXX−XXX